Chemical Science

ROYAL SOCIETY OF CHEMISTRY

EDGE ARTICLE

View Article Online
View Journal | View Issue

Cite this: *Chem. Sci.*, 2025, **16**, 17345

All publication charges for this article have been paid for by the Royal Society of Chemistry

Tuning probe permeability *via* chalcogen and halogen atom substitution for monitoring alkaline phosphatase activity in mammalian cells

Ekta Chauhan,† Debasish Giri,† Harinarayana Ungati and Govindasamy Mugesh *

Alkaline phosphatase (ALP) is a family of hydrolase enzymes that play crucial roles in a wide range of biological processes. Its primary function is to catalyze the hydrolysis of phosphate groups from various molecules, a process known as dephosphorylation. It regulates diverse cellular functions such as bone metabolism and liver function. Alteration of ALP can be a biomarker for pathological conditions. Hence, the development of fluorescent probes for ALP detection is essential for studying dynamic dephosphorylation processes in living organisms. Herein, we report a ratiometric fluorescent probe based on a 1,8-naphthalimide derivative functionalized with an ALP-reactive phosphate group and a chalcogen or halogen atom as recognition moieties to enhance the probe internalization in mammalian cells. Upon ALP-mediated cleavage of the phosphate group, the photophysical properties of these compounds undergo significant changes, enabling ratiometric fluorescence detection. Although all the synthesized compounds demonstrated excellent biocompatibility, as well as strong selectivity and sensitivity towards ALP, the selenium-based compound exhibited superior performance in cell-based studies due to its rapid cellular internalization. This compound enables monitoring of ALP activity within a shorter time frame and can be used to identify new inhibitors of ALP. Furthermore, chalcogen-containing compounds were found to be internalized by cells primarily through macropinocytosis, likely mediated by chalcogen bonding, with those capable of forming stronger chalcogen bonds demonstrating greater cellular uptake.

Received 22nd June 2025
Accepted 18th August 2025

DOI: 10.1039/d5sc04585a

rsc.li/chemical-science

Introduction

Nature's choice of phosphates as fundamental building blocks in biological systems may originate from their negative charge, hydrolytic resistance, and ability to form stable enzyme-labile linkages, making them ideal substrates for biochemical regulation.[1,2] Among phosphatase enzymes, alkaline phosphatase (ALP), a hydrolase enzyme, plays an important role in cleaving the phosphate groups from proteins, nucleic acids, and small biomolecules, thereby playing a crucial role in phosphate metabolism in living organisms.[3–5] The enzymatic reaction is facilitated by two important metal ions present in the active site: zinc (Zn^{2+}), which stabilizes the enzyme–substrate complex as well as activates the catalytic site, and magnesium (Mg^{2+}), which assists in substrate binding and product release. The reaction proceeds through a two-step mechanism, starting with the hydroxyl group of the Ser102 residue performing a nucleophilic attack on the phosphorus atom of the phosphate ester substrate, which forms a transient phospho-enzyme intermediate.[6] Subsequently, it undergoes hydrolysis, releasing free inorganic phosphate and the dephosphorylated substrate.[7–9] The enzyme is widely distributed across mammalian tissues, including the liver, kidneys, intestines, bones, and placenta, where it plays key roles in signal transduction, molecular transport, and gene regulation.[3,5,10–13] Due to its physiological significance, ALP serves as an important biomarker in clinical diagnostics, as elevated ALP levels in the bloodstream are associated with pathological conditions, such as cancer, cardiovascular disorders, bone disorders, and liver dysfunction, while reduced ALP activity may indicate metabolic disorders such as Wilson's disease.[14–17] Therefore, real-time monitoring of ALP activity is essential for understanding its physiological and pathological significance. A wide range of detection techniques—from basic colorimetric assays[18,19] to more advanced methods such as electrochemical,[20,21] chromatographic,[22] chemiluminescence,[23] and Raman spectroscopy[24]—have been developed. However, these approaches often suffer from limited sensitivity as well as the requirement of complex protocols, expensive instrumentation, or invasive sampling, thereby limiting their suitability for practical use in biological applications.

Fluorescence-based probes have been extensively used for detecting a wide range of bioanalytes, including enzymes,[25,26] small molecules,[27,28] and anions,[29,30] owing to their simplicity,

Department of Inorganic and Physical Chemistry, Indian Institute of Science, Bangalore 560012, India. E-mail: mugesh@iisc.ac.in

† These authors contributed equally.

real-time monitoring capability, high sensitivity, and non-invasive nature.[31] A variety of fluorophores, such as tetraphenylethylene,[32] naphthalimide,[33–35] coumarin,[36] and xanthene,[37,38] have been utilized in the design of ALP-responsive probes. ALP typically activates these probes through dephosphorylation, triggering a "turn-off" to "turn-on" response based on fluorescence intensity changes at a single wavelength. However, such probes are susceptible to variations in excitation intensity, emission efficiency, and probe concentration. To overcome these issues, ratiometric fluorescence probes have been developed, enabling more reliable and quantitative detection by measuring intensity ratios at two different wavelengths.[29,39–41] Although several probes are available for monitoring ALP activity, their application in cell-based studies is often limited by poor cellular uptake in mammalian cells, requiring extended incubation times for internalization. Non-covalent interactions, particularly halogen (XB) and chalcogen (ChB) bonding, have recently emerged as critical tools for applications ranging from drug design, catalysis, and probe design to anion recognition.[42–50] Matile and co-workers have developed a range of interesting synthetic systems for anion transport, such as chloride ion transport, which is specifically mediated through various types of non-covalent interactions.[51] In certain cases of anion transport, chalcogen bonding involving tellurium has been shown to be more suitable than other non-covalent interactions, such as halogen and pnictogen bonding.[52] In our recent study, we demonstrated that such interaction can also play a crucial role in facilitating the efficient cellular uptake of small molecules.[53–55] Depending on the nature of the non-covalent interaction, the molecules were internalized by the cells through distinct mechanistic pathways. In this study, we report that the cellular internalization of ALP-responsive probes in mammalian cells can be significantly enhanced through these interactions. Our systematic investigation revealed that incorporating a selenium-based recognition moiety as a chalcogen bond donor remarkably improves the cellular uptake as compared to its iodine-substituted counterpart (XB donor), resulting in a higher signal-to-noise ratio and a faster response time.

Results and discussions

Compounds **1–7** used in this study were systematically designed to have three important distinct structural features (Fig. 1A). The first component is a 1,8-naphthalimide derivative, positioned at the core of the designed molecules, serving as the fluorophore and enabling both product detection and *in situ* visualization within biological systems. The second component is a phosphate group, attached to one end of the probe, functioning as the reactive center for alkaline phosphatase (ALP). The third and most critical component is a recognition moiety, conjugated to the opposite end of the probe, and structurally varied to include substrates bearing chalcogen (**1–3**) and halogen atoms (**4**). This recognition moiety is strategically designed to promote selective interactions with the cellular membrane through non-covalent interactions, thereby enhancing the cellular uptake and improving the signal-to-noise ratio within the cellular environment (Fig. 1A). Previously, we demonstrated that the introduction of heavier halogen or chalcogen atoms significantly enhances the cellular uptake of fluorescent compounds, likely through non-covalent interactions (XB or ChB) with the cell membrane.[55] Compounds **5–7**, which lack chalcogen or halogen atoms, were included as controls to investigate the role of heavier elements in the cellular delivery (Fig. 1B). Although the tellurium-substituted compounds showed the highest uptake among chalcogen analogues, we excluded tellurium compounds from this study due to fluorescence quenching caused by the internal heavy atom effect.

Compounds **1–7** were synthesized starting from 4-bromo-1,8-naphthalic anhydride, which was reacted with various substituted anilines, including 4-(phenoxy)-aniline, 4-(phenylthio)-aniline, 4-(phenylselanyl)-aniline, 3,5-diiodo-4-methoxyaniline, aniline, 4-methoxyaniline, and ethylamine (Fig. 1C). In the subsequent step, the bromine atom at the 4-position was replaced with a hydroxyl group by using *N*-hydroxysuccinimide (NHS) and potassium carbonate. These hydroxylated derivatives were then treated with phosphorus oxychloride in pyridine, followed by hydrolysis to yield final compounds (Fig. 1C). All the final products were characterized by NMR and mass spectrometry, and purity was checked using HPLC (Fig. S33 and S34).

Density functional theory (DFT) calculations[56–58] indicate the presence of a σ-hole on the chalcogen atoms (S, Se) in compounds **2** and **3**, and on the iodine atom in compd. **4** (Fig. 1D). The strength of the σ-hole correlates directly with the strength of the resulting non-covalent interactions, such as chalcogen and halogen bonding.[42] Among compounds **1–3**, the oxygen atom in the recognition moiety of compd. **1** displays a negative electrostatic potential maximum ($V_{S,max}$) of −0.018 a.u. at the surface, indicating the absence of a significant σ-hole due to the high electronegativity of oxygen and small atomic size (Fig. 1D). In contrast, as the chalcogen atom becomes heavier, the $V_{S,max}$ becomes less negative for sulfur (compd. **2**, −0.0020 a.u.) and turns positive on the surface of the selenium (compd. **3**, 0.0035 a.u.) atom (Fig. 1D). Although the $V_{S,max}$ for sulfur is negative, it is well established that sulfur can still participate in chalcogen bonding, as donor interactions induce polarization around chalcogen bond donor, enhancing the σ-hole and facilitating bond formation.[59,60] The σ-hole on the iodine atom in compd. **4** is significantly stronger, with a ($V_{S,max}$) of 0.030 a.u. due to its high polarizability and large atomic radius compared to that of chalcogen atoms (Fig. 1D). The formation of chalcogen bond interaction in solution was confirmed *via* NMR spectroscopy. When 4-(phenylseleno)-aniline (a chalcogen bond donor) was treated with tetrabutylammonium iodide (TBAI serving as acceptors), a notable upfield shift in the ^{77}Se NMR signal was observed (Fig. 1E). This shift increases with the increase in the amount of halide concentration, providing strong evidence for the formation of chalcogen bonds in solution, which is in agreement with previous studies involving chalcogen bond donors and acceptors.[61]

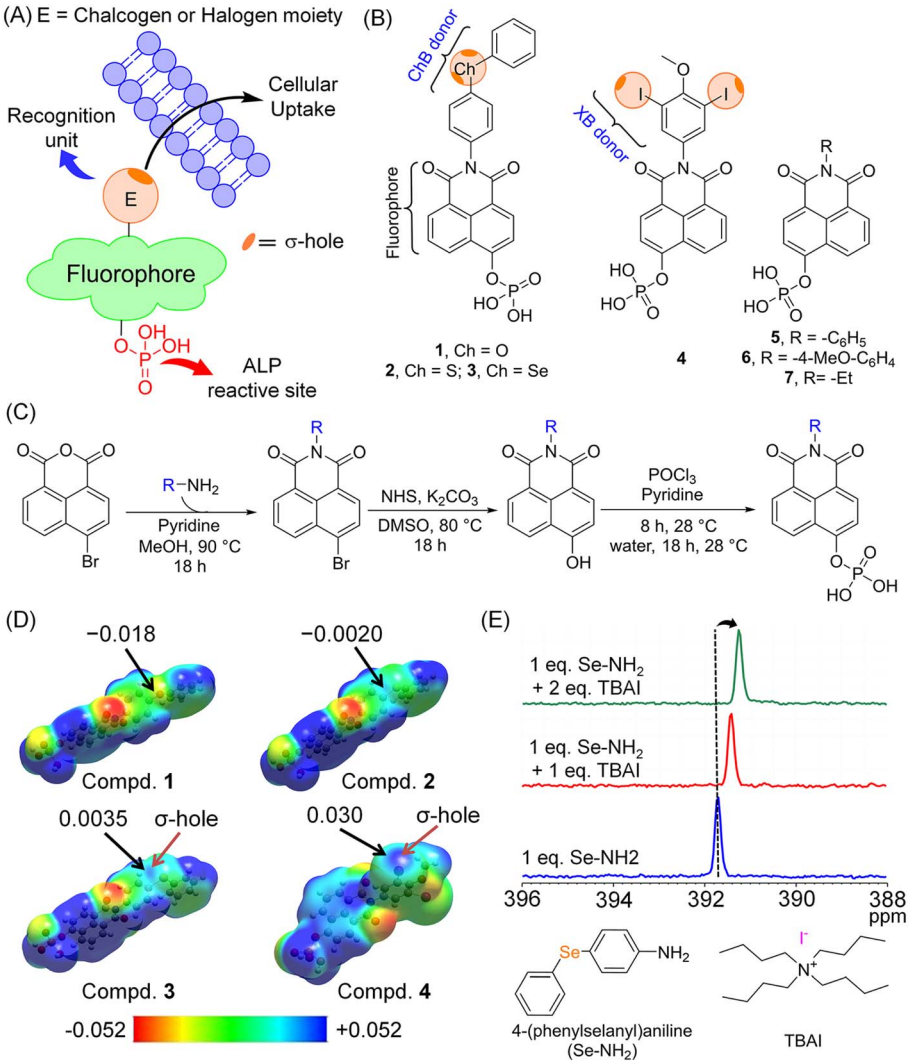

Fig. 1 (A) Design of ratiometric fluorescent compounds for monitoring ALP activity by attaching a phosphate group to a naphthalimide core along with a recognition moiety containing a σ-hole. (B) Structures of compounds **1–7** used in this study, featuring chalcogen and halogen atom substitutions. (C) General synthetic scheme for compounds **1–7** starting from 4-bromo-1,8-naphthalic anhydride. (D) Electrostatic potential (ESP) diagrams for compounds **1–4**, showing computed electrostatic potential maxima ($V_{S,max}$) at the σ-hole of chalcogen and halogen atoms (in a.u., iso value: 0.001 a.u.). (E) ^{77}Se NMR of 4-(phenylselanyl)-aniline in the presence of different concentrations of tetrabutylammonium iodide in DMSO-d_6.

Next, we evaluated alkaline phosphatase (ALP) activity by adding 0.05 U mL^{-1} ALP to a solution of compounds **1–7** in Tris-HCl buffer (pH 8.0) (Fig. 2A). Upon ALP addition, a rapid visible color change from colorless to yellow was observed within minutes under white light (Fig. 2B). This color transition was also accompanied by a red shift in the fluorescence emission from the blue to green region, indicating enzymatic activity (Fig. 2B). The enzymatic dephosphorylation reaction was confirmed by HPLC analysis using compd. **3** as a model substrate. Initially, compd. **3** showed a retention time of 15.3 min, which gradually diminished upon incubation with ALP (0.005 U mL^{-1}), accompanied by the appearance of a new peak corresponding to the dephosphorylated product, compd. **10**, having a 4-hydroxyl group (Fig. 2C). Similar reactivity was observed for other compounds when treated with ALP, showing the formation of dephosphorylated hydroxyl-containing products (**8–14**) (Fig. S35 and S36). The dephosphorylation process was further supported by ^{31}P NMR spectroscopy, which revealed the disappearance of the phosphate signal from compd. **3** alongside the appearance of a peak corresponding to that of phosphate ion (PO_4^{3-}) (Fig. 2D). These findings clearly suggest that all compounds act as efficient substrates for ALP, enabling detection of ALP activity through a simple colorimetric assay.

Next, we investigated the photophysical properties of these compounds to evaluate their suitability as fluorescent probes. Compounds **1–7** exhibited a strong absorption band near 375 nm and an emission peak at 468 nm (Fig. 2E and S37). Upon addition of 0.05 U mL^{-1} ALP in 0.1 M Tris-HCl buffer (pH 8.0), both the absorption and emission spectra underwent a significant redshift, with the absorption maximum shifting from

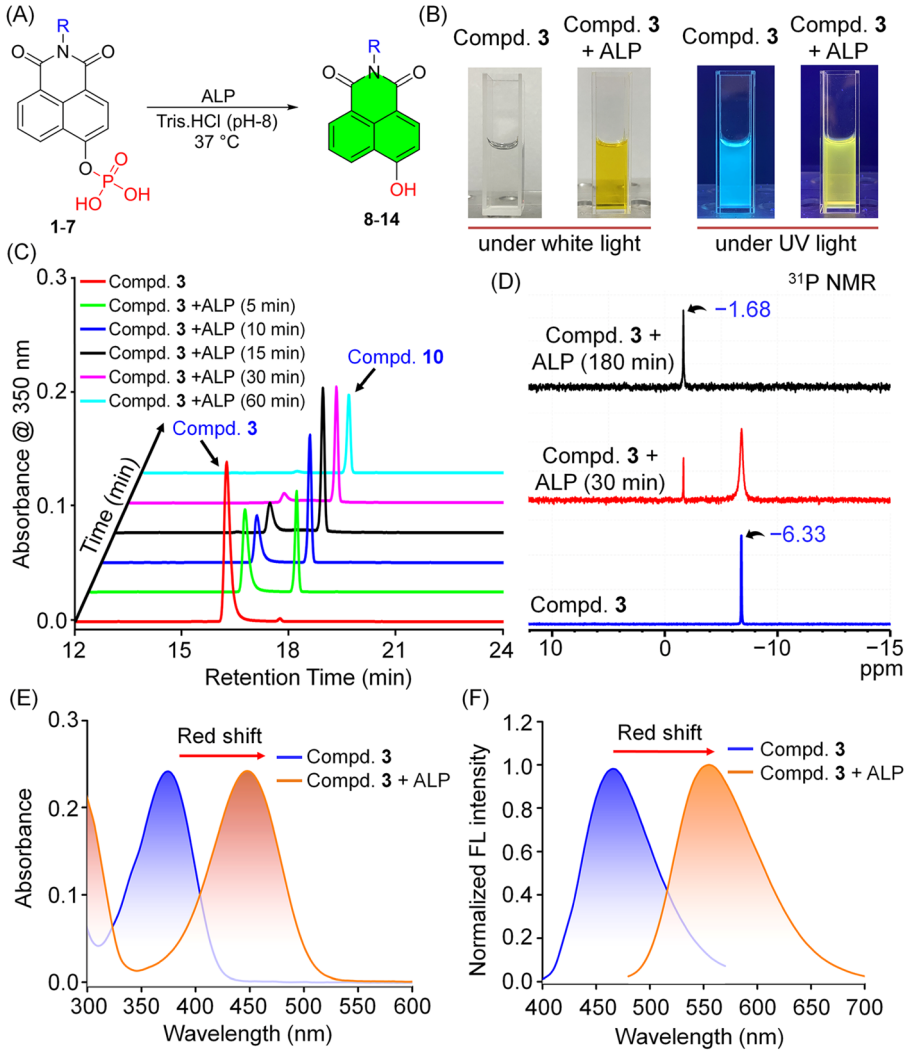

Fig. 2 (A) ALP-mediated dephosphorylation of compounds **1–7** leading to the formation of dephosphorylated products **8–14**. (B) Change in the color of compd. **3** in solution from colorless to yellow before and after ALP treatment, with a corresponding shift from blue to green fluorescence observed under UV light. (C) HPLC chromatograms of compd. **3** after incubation with ALP (0.005 U mL^{-1}) in Tris-HCl buffer (0.1 M, pH 8) at different time points, showing the formation of dephosphorylated product compd. **10**. (D) ^{31}P NMR spectra of compd. **3** before and after ALP treatment confirming the release of phosphate ion (DMSO-d_6 and D_2O mixture). (E) UV-Vis spectra of compd. **3** before and after ALP addition (0.05 U mL^{-1}) in Tris-HCl buffer (0.1 M, pH 8). (F) Normalized fluorescence spectra of compd. **3** before and after ALP addition (0.05 U mL^{-1}) in Tris-HCl buffer (0.1 M, pH 8).

375 nm to 446 nm and the emission maxima shifting from 468 nm to 556 nm, accompanied by a change in the quantum yield from 0.11 (compd. **3**) to 3.99 (compd. **10**) in Tris-HCl buffer (pH 8.0) (Fig. 2F and S38–S40). The fluorescence observed for the phosphorylated compounds arises from weak intramolecular charge transfer (ICT) between the 4-*O*-substituent linked to the phosphate group and the carbonyl group of the naphthalimide fluorophore.[34,62] However, enzymatic dephosphorylation by ALP converts the phosphate group to the hydroxyl (–OH) group, whose stronger electron-donating ability results in a dramatic shift in the fluorescence emission to a higher wavelength, and a 36-fold increase in the quantum yield was observed for compd. **3**. A similar observation was made for all the compounds in the series.

Time-course experiments using UV-Vis and fluorescence spectroscopy further confirmed the ratiometric nature of the probes. Following ALP addition, the absorption peak at 375 nm gradually decreased, while the peak at 446 nm steadily increased, indicating progressive dephosphorylation (Fig. 3A and S41). Correspondingly, the fluorescence intensity at 468 nm (associated with the phosphate form) diminished over a period of time (Fig. 3B and S40C, S42, S43), while the emission at 556 nm (corresponding to the hydroxylated form) increased proportionally, surpassing the intensity of the phosphate form (Fig. 3C and S42, S43, S40D). The reaction reached completion within ≈30 min, as no further changes in either absorption or emission intensity were observed beyond this point.

Interestingly, all the compounds except compd. **4**, which contains a 3,5-diiodo moiety, underwent nearly complete

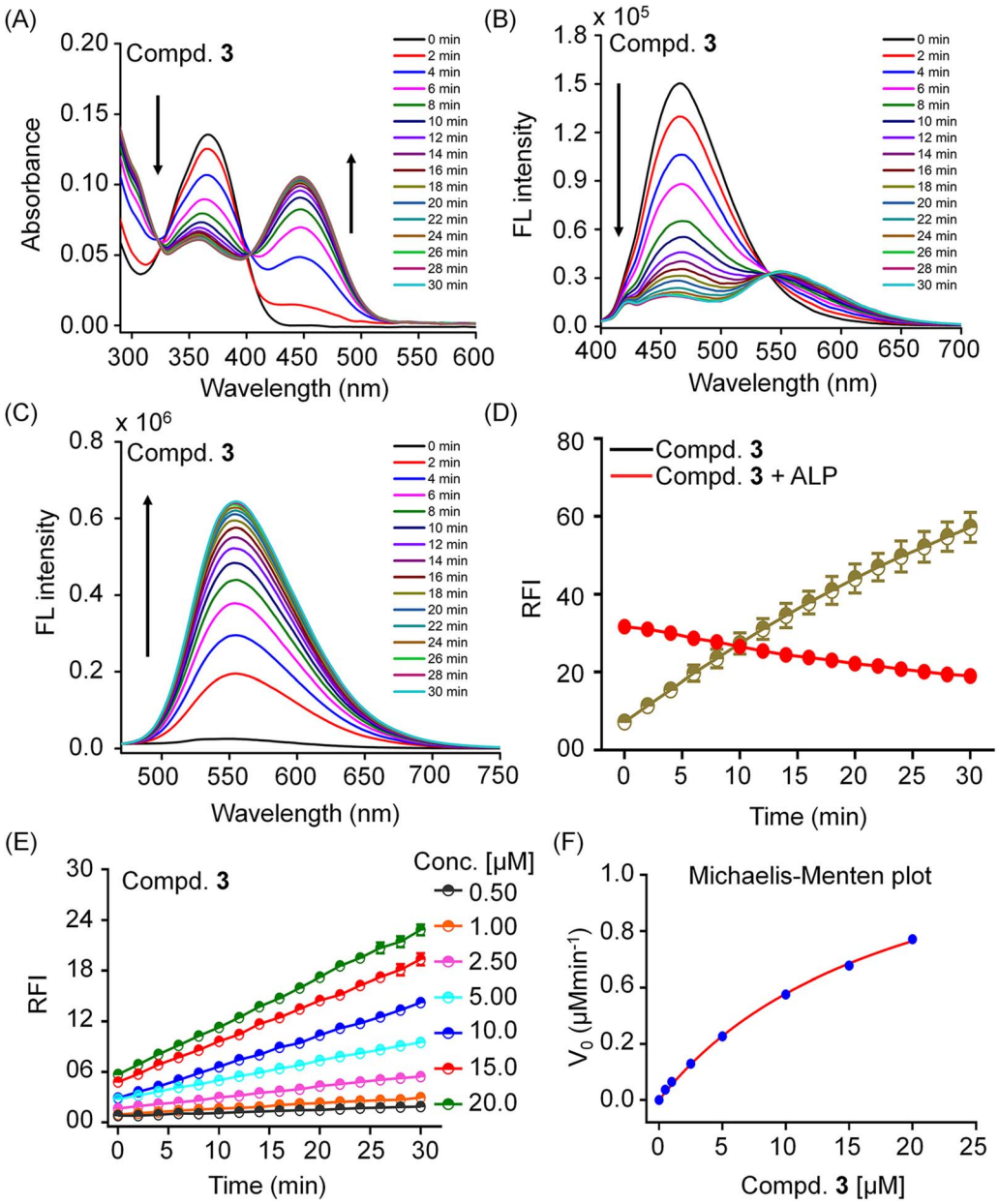

Fig. 3 (A) Time-dependent UV-Vis spectra of compd. **3** after the addition of ALP (0.05 U mL^{-1}) in Tris-HCl buffer (0.1 M, pH 8), showing a decrease in the absorption intensity of the phosphate group and a corresponding increase in the intensity of the dephosphorylated product. (B) Time-dependent fluorescence spectra of compd. **3** after the addition of ALP (0.05 U mL^{-1}) in Tris-HCl buffer (0.1 M, pH 8) showing a decrease in the fluorescence intensity of the phosphate group and a corresponding increase for the dephosphorylated product (excitation wavelength: 375 nm). (C) Time-dependent fluorescence spectra of compd. **3** after the addition of ALP (0.05 U mL^{-1}), under identical conditions (excitation wavelength: 446 nm). (D) Fluorescence intensity *vs.* time plot showing ratiometric behavior of compd. **3** (mean ± SD, $n = 3$). (E) Fluorescence intensity at 556 nm over time with varying concentrations of compd. **3** (0.5–20 μM) at fixed ALP (0.003 U mL^{-1}) (mean ± SD, $n = 3$). (F) Michaelis–Menten plot for compd. **3** (mean ± SD, $n = 3$).

conversion within the reaction timeframe (Fig. S35D). A time-dependent HPLC study further supported this observation (Fig. S44). While compd. **3** showed nearly 90% conversion to its dephosphorylated product (compd. **10**) within 30 min, a substantial portion of compd. **4** remained unconsumed, indicating a significantly slower enzymatic reaction rate (Fig. 2C). To investigate whether product inhibition might contribute to the slow conversion of compd. **4**, we evaluated the ALP activity of compd. **5** in the presence of compd. **11**, the dephosphorylated product of compd. **4**. Compd. **5** was selected for this study because its dephosphorylated product and compd. **4** exhibit distinct HPLC retention times, enabling clear separation and accurate analysis. No significant inhibition of the ALP activity was observed in the presence of compd. **11**, even at higher concentrations, suggesting that product inhibition is unlikely to happen during the hydrolysis (Fig. S45). The slow

dephosphorylation of compd. **4** is more likely due to the steric hindrance introduced by the bulky 3,5-diiodo groups, which may hinder its proper binding to the ALP active site. To further investigate the role of steric hindrance, we evaluated the activity of compd. **15**, having a 3-iodo substituent. Unlike the diiodo analogue, compd. **15** undergoes a fast and complete conversion to its dephosphorylated product, supporting the assumption that the steric effect caused by the 3,5-diiodophenyl moiety contributes to the slower reactivity of compd. **4** (Fig. S46).

While investigating the enzymatic activity of ALP on compounds **1–7** at varying ALP concentrations (0 to 0.1 U mL^{-1}) with a constant compound concentration, we observed a gradual decrease in the fluorescence intensity corresponding to the phosphate form, accompanied by a concurrent increase in the fluorescence from the hydroxylated form, which eventually surpassed that of the phosphate analogue (Fig. 3D and S47–S52). To find out the sensitivity of compounds **1–7** towards ALP, we analyzed the fluorescence intensity ratio (F_{556}/F_{468}) as a function of ALP concentration. A strong linear relationship was observed between the fluorescence ratio and ALP concentrations ranging from 0 to 0.1 U mL^{-1}, within a shorter reaction time (Fig. S53 and S54). The seven compounds exhibited excellent sensitivity for ALP detection with limits of detection ranging from 0.0022 to 0.0001 U mL^{-1}, well below the physiological ALP concentration, making them highly suitable for biological assays.[63] To evaluate the interaction between ALP and the synthesized probes, key kinetic parameters (K_M, V_{max}, K_{cat}, and K_{cat}/K_M) were determined and are summarized in Table 1. The fluorescence responses of compounds **1–7** were analyzed over a concentration range of 0.5–20 μM in the presence of 0.003 U mL^{-1} ALP (Fig. 3E and S55), with measurements recorded over a 30 minutes reaction time. Kinetic parameters were calculated using Lineweaver–Burk plots (Fig. 3F and S56, S57). The K_M values for compounds **2**, **3**, and **4** were 6.86 μM, 7.61 μM, and 2.74 μM, respectively, indicating good affinity for ALP. The value of K_{cat}/K_M of synthesized probes was found to be higher than that of two commercial ALP probes, 4-MUP ($K_{cat}/K_M = 7.7 \times 10^3$ M^{-1} s^{-1}) and ELF-97 ($K_{cat}/K_M = 3.0 \times 10^4$ M^{-1} s^{-1}), indicating a high catalytic efficiency of ALP toward the compounds.[37] Among all the probes, compd. **4** showed the highest catalytic efficiency ($K_{cat}/K_M = 1.09 \times 10^6$ $M^{-1}s^{-1}$), while compd. **7** exhibited the lowest (1.31×10^5 $M^{-1}s^{-1}$). This analysis indicates that the substituents do not significantly influence ALP activity, as they are located away from the ALP-reactive site and have no strong electronic communications with the phosphoester bond. Compd. **7**, containing an ethyl group, was not studied further as it is expected to have limited cellular uptake and lower affinity and catalytic efficiency toward ALP, as suggested by its high K_M and low K_{cat}/K_M value.

The specificity of compounds **1–6** was evaluated against various biologically relevant analytes present in the cells, including amino acids such as cysteine and homocysteine and peptide-based thiol glutathione (GSH), as well as different proteins. Upon treatment with ALP, the fluorescence signals of the test compounds increased significantly, while no noticeable changes were observed in the presence of other analytes (Fig. 4A and S58). Similarly, when incubated with various enzymes, including esterase, trypsin, papain, catalase, and lysozyme, no significant fluorescence changes were detected (Fig. 4A and S58). These results clearly demonstrate that the compounds exhibit high specificity and selectivity toward ALP, making them well-suited for biological applications.

Given the dynamic and variable nature of intracellular environments, assessing the stability and performance of fluorescent probes across different pH conditions is essential. Compounds **1–6** showed relatively weak fluorescence over a broad pH range (3.0–10.0) with minimal intensity changes. Upon addition of ALP, the fluorescence intensity strongly depended on the pH of the solution, reaching a maximum at pH 7.0 (Fig. 4B and S59). This indicates that the probe is most effective under slightly alkaline conditions, particularly at pH > 6. Further analysis revealed that the fluorescence enhancement at higher pH is not solely due to increased enzymatic activity but also results from the formation of the hydroxylate anion derived from the hydroxy product (Fig. 4C). Notably, the fluorescence intensity of compd. **10** increased drastically at pH values above 6.0 (Fig. 4D). Formation of the strongly electron-donating hydroxylate anion enhances intramolecular charge transfer, leading to a redshift and a significant increase in fluorescence, as supported by TD-DFT calculations.[56–58] In these compounds, the LUMO is mostly localized on the naphthalimide moiety. For compd. **3**, the HOMO is on the phenyl ring having selenium, and the HOMO → LUMO transition is symmetry-forbidden ($f = 0$) (Fig. 4E). The allowed transition occurs from HOMO−1 to LUMO ($f = 0.39$) (Fig. 4E). A similar observation was found in compd. **10** having a hydroxyl group, with a decrease in the transition energy as compared to that of the corresponding phosphate compound. In contrast, in the hydroxylated compound, the deprotonation shifts the dominant transition to HOMO → LUMO, both localized on the naphthalimide moiety,

Table 1 Key kinetic parameters K_M, V_{max}, K_{cat}, and K_{cat}/K_M

Compds	K_M (μM)	V_{max} (μM min^{-1})	K_{cat} (s^{-1})	K_{cat}/K_M (M^{-1} s^{-1})	LOD (U mL^{-1})
1	9.37	0.791	7.03	7.50×10^5	0.0010
2	6.86	0.713	6.34	9.25×10^5	0.0004
3	7.61	0.591	5.25	6.90×10^5	0.0009
4	2.74	0.336	2.99	1.09×10^6	0.0015
5	8.81	0.798	7.11	8.05×10^5	0.0022
6	8.97	0.841	7.47	8.33×10^5	0.0003
7	10.51	6.91	1.38	1.31×10^5	0.0001

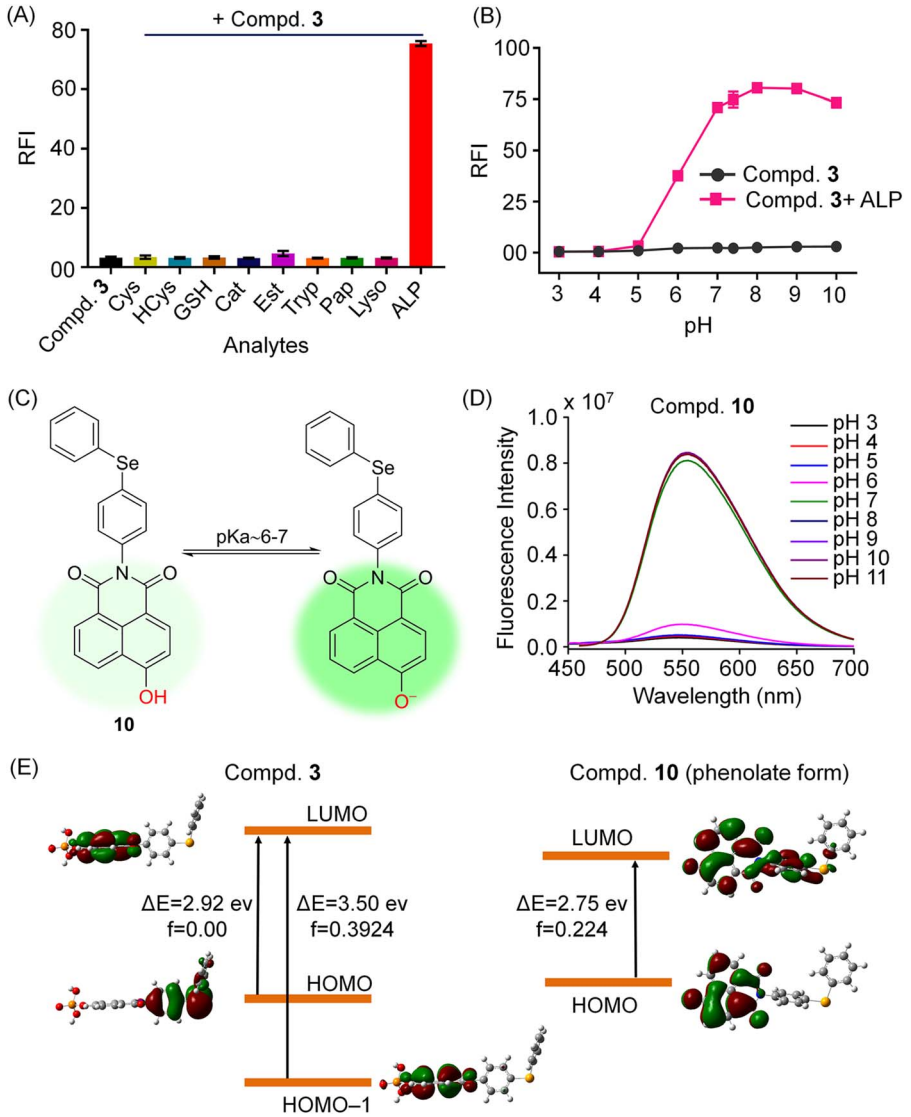

Fig. 4 (A) Fluorescence response of compd. **3** (10 μM) in the presence of some biologically relevant analytes in Tris-HCl buffer (excitation at 444 nm). The data are represented as the mean ± SD ($n = 3$). (B) Changes in the fluorescence intensity of compd. **3** in the absence and presence of ALP under varying pH conditions (pH 3–10). The data are represented as the mean ± SD ($n = 3$). (C) Chemical structure of the compd. **10** showing protonated and deprotonated form. (D) Fluorescence intensity of compd. **10** (10 μM) at different pH conditions (pH 3–10). (E) Calculated orbital energy levels and electron density contours of the HOMO, HOMO−1, and LUMO for compounds **3** and **10** (in deprotonated form).

lowering the transition energy and indicating stronger charge transfer (Fig. 4E). Experimentally, this correlates well with a 36-fold increase in the quantum yield for the hydroxylated compound, reflecting enhanced charge transfer and fluorescence efficiency. In addition to their pH stability, compounds **1–6** demonstrated excellent photostability (Fig. S60), showing only minimal fluorescence intensity loss over prolonged light exposure. This robustness is crucial for long-term imaging applications that require repeated excitation and emission cycles without significant loss of signal.

To determine the suitable concentrations of compounds to be used for the cellular uptake studies, cell viability assays were carried out in HepG2 (human liver carcinoma) cells at different concentrations of compounds **1–6** (Fig. 5A). This indicates that these compounds are non-toxic up to a concentration of 25 μM after incubation for 12 h. All the compounds exhibited similar cytotoxicity profiles irrespective of the nature of chalcogen or halogen atom substitution (Fig. 5A). Therefore, a concentration of 10 μM was selected for all compounds in cellular uptake experiments, which were performed in HepG2 and HeLa cell lines, known to express alkaline phosphatase (ALP).[64,65] The cellular uptake studies were monitored through laser scanning microscopy and quantified through flow cytometry. After a 15 minutes incubation at a concentration of 10 μM in HepG2 cells, confocal microscopy and flow cytometry confirmed that these compounds underwent ALP-mediated dephosphorylation as indicated by the appearance of fluorescence corresponding to the dephosphorylated products (Fig. 5B). Notably, the fluorescence intensity strongly depends on the nature of the chalcogen or halogen substituent present in the compound. The selenium-

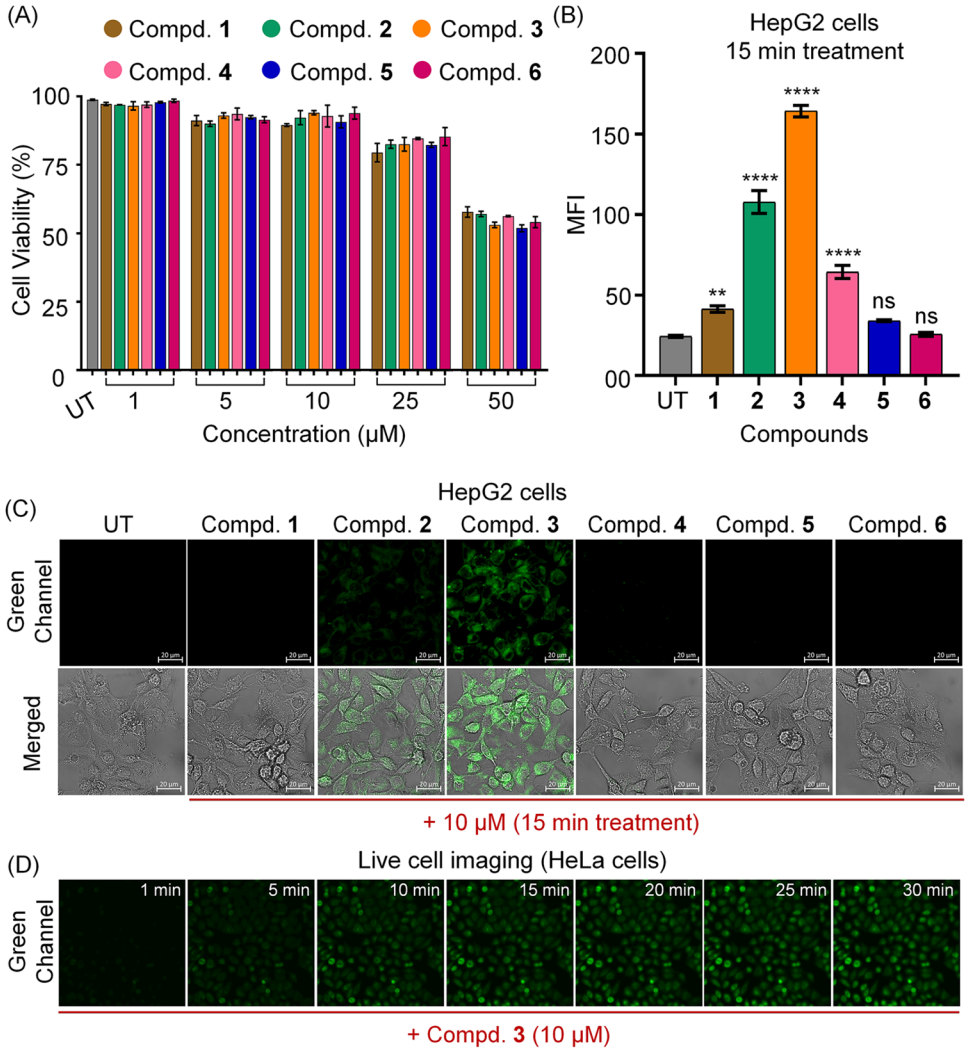

Fig. 5 (A) Cell viability of HepG2 cells treated with different concentrations of compounds **1–6** for 12 h. The data are represented as mean ± SD ($n = 5$). (B) Mean fluorescence intensity (MFI) measured by flow cytometer after treating HepG2 cells with compounds **1–6** (10 μM) for 15 min. The data are represented as mean ± SD ($n = 3$), $^{**}p < 0.01$, $^{****}p < 0.0001$, significant compared to UT (untreated) cells. (C) Confocal microscopy images of HepG2 cells treated with compounds **1–6** (10 μM) for 15 min. (D) Time-course fluorescence images of HeLa cells treated with compd. **3** (10 μM) for different times.

containing probe compd. **3** exhibited the highest intracellular fluorescence, followed by sulfur (compd. **2**) and iodine-based (compd. **4**) compounds (Fig. 5B, C and S61). These differences in the observed intensity can be ascribed primarily to the variations in the cellular uptake efficiency rather than their enzymatic reactivity, as all the compounds show almost similar reactivity towards ALP *in vitro*. Furthermore, in Tris-HCl buffer, the iodine-containing hydroxylated compd. **11** exhibited fluorescence intensity comparable to that of the selenium analogue (compd. **10**) (Fig. S62A). This suggests that the differences in the cellular fluorescence arise mainly from the variations in the cellular uptake, with the selenium compound being taken up at a much faster rate. Compounds **5** and **6**, which lack any halogen or chalcogen functionality, showed significantly lower fluorescence, suggesting poor cellular uptake (Fig. 5C).

Our observations suggest that incorporating chalcogen atoms into ALP fluorescent probes significantly enhances their cellular internalization rate. Among the substitutions, the selenium-containing compounds exhibited the highest uptake compared to their oxygen and sulfur analogues. This superior uptake is likely attributed to the deeper σ-hole of the selenium atom, which facilitates stronger non-covalent interactions (chalcogen bonds) with the cell membrane. Based on our DFT computational studies, compd. **4** having a halogen atom, would be expected to show a higher rate of cellular uptake due to stronger halogen-bond interactions. However, we observe lower fluorescence intensity, which can be explained by a slower enzymatic reaction rate or a relatively lower abundance of specific transporters responsible for the uptake of compd. **4**. When the cellular uptake of compounds **1**, **4**, and **6** was compared, it was observed that compd. **4** exhibited a slightly higher uptake than the other two compounds (Fig. S62B). A similar uptake trend was seen in HeLa cells, where compd. **3** once again showed the strongest fluorescence signal, following

ALP-mediated conversion (Fig. S63). These results clearly highlight compd. **3** as the most promising candidate for real-time ALP imaging in mammalian cells due to its superior uptake. Time-dependent studies in HeLa and HepG2 cells showed fluorescence signals within 2 min of incubation with signal intensity increasing gradually over time, confirming rapid cellular internalization and conversion (Fig. 5D and S64, S65).

To evaluate the potential of compounds **1–6** for screening ALP inhibitors, their response to sodium orthovanadate (Na_3VO_4), a known competitive ALP inhibitor, was tested.[5] Fluorescence measurements after preincubation with inhibitor showed a concentration-dependent decrease in signal, with maximal inhibition at 5 mM Na_3VO_4, confirming their selectivity toward ALP (Fig. 6A and S66). Specifically, compd. **3** exhibited concentration-dependent inhibition with an IC_{50} value of 10.2 μM, consistent with the previously reported findings (Fig. 6A).[66] Cell-based assays in HepG2 and HeLa cells showed that co-treatment with Na_3VO_4 and compd. **3** significantly reduced the intracellular fluorescence compared to cells treated with compd. **3** alone (Fig. 6B, C and S67). This confirms that the probe can be used to monitor ALP activity in live cells and highlights its potential role for identifying novel ALP inhibitors. Similarly, we further assessed its selectivity in different cell lines with varying ALP expression levels. HEK 293T cells, known for low ALP expression, were compared with HeLa and HepG2 cells, which exhibit higher ALP levels.[64,67] Following 15 min of incubation with 10 μM of the probe and thorough washing, fluorescence imaging showed the strongest signal in HepG2 cells, slightly lower intensity in HeLa, and minimal fluorescence in HEK 293T (Fig. 6D and S68). These results are in excellent correlation with the known ALP expression profiles, confirming the potential of the new probe for monitoring ALP activity across different cell types.

Finally, we explored the cellular uptake pathway of compd. **3** using different cellular uptake inhibitors. A significant decrease in the intracellular fluorescence was observed when the cells were treated with rottlerin (ROTN), an inhibitor of micropinocytosis (Fig. 6E and S70).[68–70] ROTN blocks this pathway by inhibiting protein kinase C delta (PKCδ), which plays a role in actin cytoskeleton remodelling through downstream effectors such as cofilin.[71] This suggests that compd. **3** is likely taken up *via* micropinocytosis, as previously reported for the cellular uptake of a series of selenium-based compounds.[55] In contrast, no change in the fluorescence intensity was observed upon treatment with silychristin (SY), an MCT8 (monocarboxylate transporter 8) inhibitor (Fig. 6E and S70),[72] whereas compd. **4**, which contains two iodine atoms, showed reduced uptake when

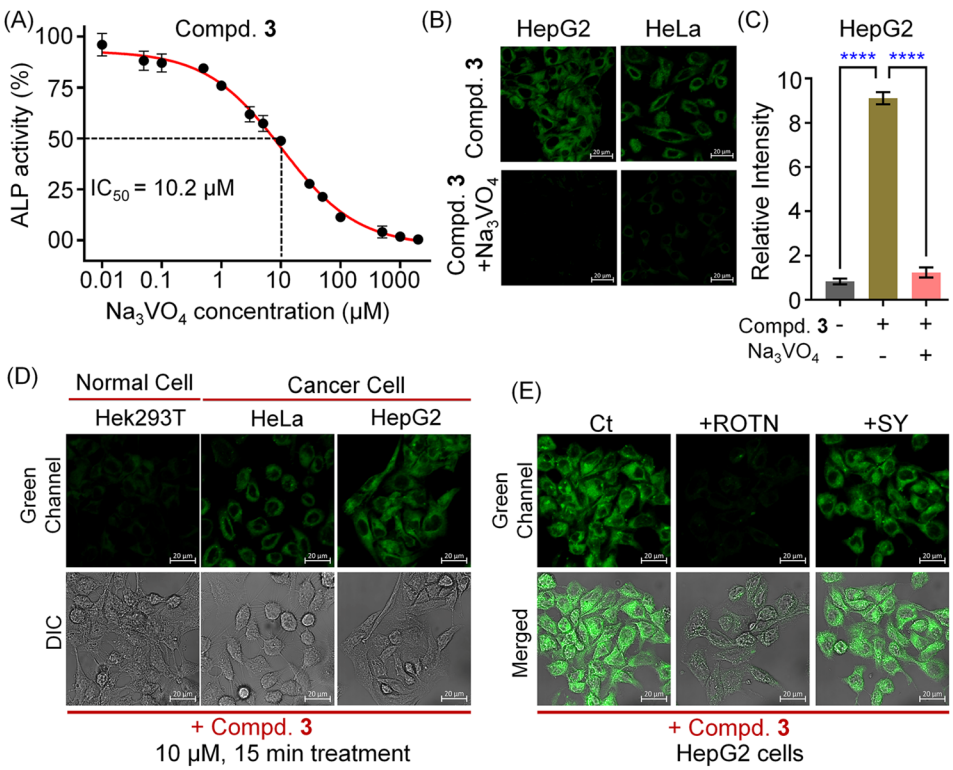

Fig. 6 (A) Percentage of ALP activity of compd. **3** in the presence of varying concentrations of the inhibitor sodium orthovanadate. Data are presented as mean ± SD ($n = 3$). (B) Confocal microscopy images of HepG2 and HeLa cells treated with compd. **3** (10 μM) for 15 minutes, in the presence and absence of sodium orthovanadate (5 mM). For the inhibition study, compd. **3** and sodium orthovanadate were co-incubated for 15 min. (C) The relative fluorescence intensity of compd. **3** in the presence of sodium orthovanadate (5 mM) after a treatment. The data are represented as the mean ± SD ($n = 3$); ****$p < 0.0001$, significant compared to UT (untreated) cells and treated cells. (D) Confocal microscopy images of HEK293T, HeLa, and HepG2 cells treated with compd. **3** (10 μM) for 15 min. (E) Fluorescence microscopy images of HepG2 cells treated with compd. **3** (10 μM) for 15 min after pre-treatment with rottlerin (30 μM) and silychristin (100 μM) for 30 min.

treated with SY or ROTN (Fig. S69 and S70). This suggests a dual uptake mechanism for the iodine-based compound, involving both macropinocytosis and MCT8-mediated transport. These observations align with previous reports indicating that iodine-containing molecules were taken up *via* MCT8.[73]

Conclusions

In summary, we developed a series of ratiometric fluorescent probes capable of effectively monitoring alkaline phosphatase (ALP) activity in mammalian cells with high sensitivity and selectivity. These compounds exhibit distinct absorption and emission changes upon enzymatic activation, enabling clear differentiation between phosphorylated and dephosphorylated forms. A novel finding of this study is the impact of structural modifications, specifically the incorporation of chalcogen and halogen atoms, on the cellular uptake. Probes containing chalcogen atoms, particularly selenium, demonstrated significantly enhanced membrane permeability compared to their halogenated counterparts, including an iodine-substituted analogue. This study suggests that incorporating a selenium-based recognition moiety can significantly enhance the sensitivity of the probe toward biological analytes by facilitating faster cellular internalization. While many ALP detection probes are available, our study introduces a novel concept that the incorporation of chalcogen atoms greatly improves the cellular uptake of ALP probes and enhances the detection sensitivity. This approach may serve as a general strategy to enhance the cellular delivery of small molecules, probes, and drugs, with broad implications for biological and biomedical applications.

Author contributions

E. C. and D. G. contributed equally to this work. E. C., D. G., and H. U. carried out the synthesis and characterization of the compounds. E. C. also performed the enzymatic assays and photophysical studies. D. G. conducted the biological experiments, designed the study, and drafted the manuscript. G. M. supervised the project, secured funding, and edited the final manuscript. All authors discussed the results and contributed to the final version of the manuscript.

Conflicts of interest

The authors declare no conflict of interest.

Data availability

Supplementary information: All experimental procedures, characterization data, HPLC chromatograms, and coordinates of optimized geometries are available in the SI. See DOI: **https://doi.org/10.1039/d5sc04585a**.

Acknowledgements

This study was supported by the Science and Engineering Research Board (JBR-2020-000003 and CRG/2022/008475). E. C. acknowledges INSPIRE and D. G. acknowledges the Indian Institute of Science, Bangalore, for a research fellowship.

Notes and references

1 F. Westheimer, *Science*, 1987, **235**, 1173–1178.
2 S. C. Kamerlin, P. K. Sharma, R. B. Prasad and A. Warshel, *Q. Rev. Biophys.*, 2013, **46**, 1–132.
3 J. E. Coleman, *Annu. Rev. Biophys. Biomol. Struct.*, 1992, **21**, 441–483.
4 N. K. Tonks, *Nat. Rev. Mol. Cell Biol.*, 2006, **7**, 833–846.
5 U. Sharma, D. Pal and R. Prasad, *Indian J. Clin. Biochem.*, 2014, **29**, 269–278.
6 S. L. Chen and R. Z. Liao, *ChemPhysChem*, 2014, **15**, 2321–2330.
7 J. L. Millan, *Purinergic Signalling*, 2006, **2**, 335–341.
8 E. E. Kim and H. W. Wyckoff, *J. Mol. Biol.*, 1991, **218**, 449–464.
9 K. M. Holtz and E. R. Kantrowitz, *FEBS Lett.*, 1999, **426**, 7–11.
10 D. J. Goldstein, C. E. Rogers and H. Harris, *Proc. Natl. Acad. Sci. U. S. A.*, 1980, **77**, 2857–2860.
11 G. Kasarala and H. L. Tillmann, *Clin. Liver Dis.*, 2016, **8**, 13–18.
12 Y. K. Liu, T. Uemura, A. Nemoto, T. Yabe, N. Fujii, T. Ushida and T. Tateishi, *FEBS Lett.*, 1997, **420**, 112–116.
13 B. L. Vinh, Z. B. A. Dağdeviren, N. M. N. Le, I. Nazir and A. B. Schnürch, *Adv. Ther.*, 2022, **5**, 2100219.
14 C. Huggins and C. V. Hodges, *Ca-Cancer J. Clin.*, 1972, **22**, 232–240.
15 M. Haarhaus, V. Brandenburg, K. K. Zadeh, P. Stenvinkel and P. Magnusson, *Nat. Rev. Nephrol.*, 2017, **13**, 429–442.
16 S. Vimalraj, *Gene*, 2020, **754**, 144855.
17 K. Ooi, K. Shiraki, Y. Morishita and T. Nobori, *J. Clin. Lab. Anal.*, 2007, **21**, 133–139.
18 Z. Gao, K. Deng, X.-D. Wang, M. Miró and D. Tang, *ACS Appl. Mater. Interfaces*, 2014, **6**, 18243–18250.
19 Z. Zhang, Z. Chen, S. Wang, F. Cheng and L. Chen, *ACS Appl. Mater. Interfaces*, 2015, **7**, 27639–27645.
20 T. Balbaied and E. Moore, *Biosensors*, 2019, **9**, 102.
21 S. Goggins, C. Naz, B. J. Marsh and C. G. Frost, *Chem. Commun.*, 2015, **51**, 561–564.
22 C. H. Zhou, J. Y. Zhao, D. W. Pang and Z. L. Zhang, *Anal. Chem.*, 2018, **90**, 6339–6345.
23 X. Liu, N. Fan, L. Wu, C. Wu, Y. Zhou, P. Li and B. Tang, *Chem. Commun.*, 2018, **54**, 12479–12482.
24 C. Ruan, W. Wang and B. Gu, *Anal. Chem.*, 2006, **78**, 3379–3384.
25 X. Wu, W. Shi, X. Li and H. Ma, *Acc. Chem. Res.*, 2019, **52**(7), 1892–1904.
26 X. Wu, R. Wang, N. Kwon, H. Ma and J. Yoon, *Chem. Soc. Rev.*, 2022, **51**, 450–463.
27 Y. Fu and N. S. Finney, *RSC Adv.*, 2018, **8**, 29051–29061.

28 J. V. Jun, D. M. Chenoweth and E. J. Petersson, *Org. Biomol. Chem.*, 2020, **18**, 5747–5763.
29 M. H. Lee, J. S. Kim and J. L. Sessler, *Chem. Soc. Rev.*, 2015, **44**, 4185–4191.
30 S. H. Park, N. Kwon, J. H. Lee, J. Yoon and I. Shin, *Chem. Soc. Rev.*, 2020, **49**, 143–179.
31 X. Tian, L. C. Murfin, L. Wu, S. E. Lewis and T. D. James, *Chem. Sci.*, 2021, **12**, 3406–3426.
32 J. Liang, R. T. K. Kwok, H. Shi, B. Z. Tang and B. Liu, *ACS Appl. Mater. Interfaces*, 2013, **5**, 8784–8789.
33 X. F. Hou, Q. X. Yu, Q. F. Zeng, J. H. Ye and S. Z. J. Wu, *J. Mater. Chem. B*, 2015, **3**, 1042–1048.
34 C. Gao, S. Zang, L. Nie, Y. Tian, R. Zhang, J. Jing and X. Zhang, *Anal. Chim. Acta*, 2019, **1066**, 131–135.
35 X. Huang, X. Chen, S. Chen, X. Zhang, L. Wang, S. Hou and X. Ma, *Spectrochim. Acta, Part A*, 2021, **260**, 119953.
36 J. Chen, J. Li, Z. Zhang, Y. Cheng, Z. Wang, X. Chen, M. She, X. Xie, P. Liu, F. Chen, S. Zhang and J. Li, *Sens. Actuators, B*, 2024, **413**, 135896.
37 Y. Tan, L. Zhang, K. H. Man, R. Peltier, G. Chen, H. Zhang, L. Zhou, F. Wang, D. Ho, S. Q. Yao, Y. Hu and H. Sun, *ACS Appl. Mater. Interfaces*, 2017, **9**, 6796–6803.
38 S. J. Li, C. Y. Li, Y. F. Li, J. Fei, P. Wu, B. Yang, J. Ou Yang and S. X. Nie, *Anal. Chem.*, 2017, **89**, 6854–6860.
39 J. Fan, M. Hu, P. Zhan and X. Peng, *Chem. Soc. Rev.*, 2013, **42**, 29–43.
40 R. Gui, H. Jin, X. Bu, Y. Fu, Z. Wang and Q. Liu, *Coord. Chem. Rev.*, 2019, **383**, 82–103.
41 Y. A. Feng, H. Xu, Y. Zhou, B. J. Wang, J. Xiao, Y. W. Wang and Y. Peng, *Sens. Actuators, B*, 2022, **358**, 131505.
42 G. Cavallo, P. Metrangolo, R. Milani, T. Pilati, A. Priimagi, G. Resnati and G. Terraneo, *Chem. Rev.*, 2016, **116**, 2478–2601.
43 P. Auffinger, F. A. Hays, E. Westhof and P. S. Ho, *Proc. Natl. Acad. Sci. U. S. A.*, 2004, **101**, 16789–16794.
44 D. J. Pascoe, K. B. Ling and S. L. Cockroft, *J. Am. Chem. Soc.*, 2017, **139**, 15160–15167.
45 L. Vogel, P. Wonner and S. M. Huber, *Angew. Chem., Int. Ed.*, 2019, **58**, 1880–1891.
46 O. Carugo, G. Resnati and P. Metrangolo, *ACS Chem. Biol.*, 2021, **16**, 1622–1627.
47 T. Bunchuay, A. Docker, U. Eiamprasert, P. Surawatanawong, A. Brown and P. D. Beer, *Angew. Chem., Int. Ed.*, 2020, **59**, 12007–12012.
48 M. Macchione, A. Goujon, K. Strakova, H. V. Humeniuk, G. Licari, E. Tajkhorshid, N. Sakai and S. Matile, *Angew. Chem., Int. Ed.*, 2019, **58**, 15752–15756.
49 A. V. Jentzsch, D. Emery, J. Mareda, S. K. Nayak, P. Metrangolo, G. Resnati, N. Sakai and S. Matile, *Nat. Commun.*, 2012, **3**, 905.
50 R. Hein, A. Docker, J. J. Davis and P. D. Beer, *J. Am. Chem. Soc.*, 2022, **144**, 8827–8836.
51 S. Benz, M. Macchione, Q. Verolet, J. Mareda, N. Sakai and S. Matile, *J. Am. Chem. Soc.*, 2016, **138**, 9093–9096.
52 L. M. Lee, M. Tsemperouli, A. I. Poblador-Bahamonde, S. Benz, N. Sakai, K. Sugihara and S. Matile, *J. Am. Chem. Soc.*, 2019, **141**, 810–814.
53 H. Ungati, V. Govindaraj and G. Mugesh, *Angew. Chem., Int. Ed.*, 2018, **57**, 8989–8993.
54 D. Giri, V. Govindaraj, S. Kumar, H. Ungati and G. Mugesh, *Chem.–Eur. J.*, 2024, **30**, e202401719.
55 E. Chauhan, D. Giri and V. Govindaraj, *Angew. Chem., Int. Ed.*, 2025, e202511786.
56 M. J. Frisch *et al.*, *Gaussian 03, Revision C.02*, Gaussian, Inc., Wallingford CT, 2004.
57 A. D. Becke, *J. Chem. Phys.*, 1993, **98**, 5648–5652.
58 E. D. Glendening, J. K. Badenhoop, A. E. Reed, J. E. Carpenter, J. A. Bohmann, C. M. Morales, C. R. Landis and F. Weinhold, *NBO 6.0*, Theoretical Chemistry Institute, University of Wisconsin, Madison, 2013.
59 A. Pizzi, A. Dhaka, R. Beccaria and G. Resnati, *Chem. Soc. Rev.*, 2024, **53**, 6654–6674.
60 A. Dhaka, R. Beccaria, A. Pizzi, E. Y. Tupikina, V. Y. Kukushkin and G. Resnati, *Chem.–Eur. J.*, 2025, **31**, e202404570.
61 A. Daolio, P. Scilabra, M. E. Di Pietro, C. Resnati, K. Rissanen and G. Resnati, *New J. Chem.*, 2020, **44**, 20697–20703.
62 H. Q. Dong, T. B. Wei, X. Q. Ma, Q. Y. Yang, Y. F. Zhang, Y. J. Sun, B. B. Shi, H. Yao, Y. M. Zhang and Q. Lin, *J. Mater. Chem. C*, 2020, **8**, 13501–13529.
63 T. Hausamen, R. Helger, W. Rick and W. Cross, *Clin. Chim. Acta*, 1967, **15**, 241–245.
64 F. Herz, *Experientia*, 1985, **41**, 1357–1361.
65 F. J. Benham and H. Harris, *Proc. Natl. Acad. Sci. U. S. A.*, 1979, **76**, 4016–4019.
66 H. Zhang, C. Xu, J. Liu, X. Li, L. Guo and X. Li, *Chem. Commun.*, 2015, **51**, 7031–7034.
67 F. Schmid, R. Fliegert, T. Westphal, A. Bauche and A. H. Guse, *J. Biol. Chem.*, 2012, **287**, 32525–32534.
68 X. Sewald, L. Jiménez-Soto and R. Haas, *Cell. Microbiol.*, 2011, **13**, 482–496.
69 V. Jayashankar and A. L. Edinger, *Nat. Commun.*, 2020, **11**, 1121.
70 Y. L. Kang, C. Oh, S. H. Ahn, J. C. Choi, H. Y. Choi and S. W. Lee, *Antiviral Res.*, 2021, **195**, 105191.
71 Y. Kang, J. C. Choi, J. B. Lee, S. Y. Park and C. Oh, *PLoS One*, 2025, **20**, e0324500.
72 J. Johannes, R. Jayarama-Naidu, F. Meyer, E. K. Wirth, U. Schweizer, L. Shomburg, J. Köhrle and K. Renko, *Endocrinology*, 2016, **157**, 1694–1701.
73 H. Ungati, V. Govindaraj, C. R. Nair and G. Mugesh, *Chem.–Eur. J.*, 2019, **25**, 3391–3399.